inorganics

MDPI

Article

Reversible Conversion between Lithium Superoxide and Lithium Peroxide: A Closed "Lithium–Oxygen" Battery

Junkai Wang [1], Rui Gao [1] and Xiangfeng Liu [1,2,*]

[1] College of Materials Science and Opto-Electronic Technology, University of Chinese Academy of Sciences, Beijing 100049, China
[2] CAS Center for Excellence in Topological Quantum Computation, University of Chinese Academy of Sciences, Beijing 100190, China
* Correspondence: liuxf@ucas.ac.cn

Abstract: Lithium–air batteries have become a desirable research direction in the field of green energy due to their large specific capacity and high energy density. The current research mainly focuses on an open system continuously supplying high-purity oxygen or air. However, factors such as water and CO_2 in the open system and liquid electrolytes' evaporation will decrease battery performance. To improve the practical application of lithium–air batteries, developing a lithium–oxygen battery that does not need a gaseous oxygen supply is desirable. In this study, we designed a closed lithium–oxygen battery model based on the conversion of lithium superoxide and lithium peroxide ($LiO_2 + e^- + Li^+ \leftrightarrow Li_2O_2$). Herein, the Pd-rGO as a catalyst will produce the LiO_2 in the pre-discharge process, and the closed battery can cycle over 57 cycles stably. In addition to in situ Raman spectra, electrochemical quartz crystal microbalance (EQCM) and differential electrochemical mass spectrometry (DEMS) have been applied to explanation the conversion between LiO_2 and Li_2O_2 during the charge–discharge process. This work paves the way to introduce a new closed "lithium–oxygen" battery system for developing large-capacity green energy.

Keywords: lithium–oxygen battery; lithium superoxide; lithium peroxide; electrochemical quartz crystal microbalance; differential electrochemical mass spectrometry

Citation: Wang, J.; Gao, R.; Liu, X. Reversible Conversion between Lithium Superoxide and Lithium Peroxide: A Closed "Lithium–Oxygen" Battery. *Inorganics* **2023**, *11*, 69. https://doi.org/10.3390/ inorganics11020069

Academic Editor: Torben R. Jensen

Received: 5 December 2022
Revised: 26 January 2023
Accepted: 29 January 2023
Published: 1 February 2023

1. Introduction

Among the various battery types, the lithium–oxygen battery is considered a promising energy storage element due to its high theoretical capacity and energy density [1–4]. However, lithium–oxygen batteries have suffered from critical issues, such as sluggish oxygen reduction/evolution reaction (ORR/OER) kinetics, high overpotential, and limited cycle life. Currently, most research about lithium–oxygen batteries has found that a high-purity oxygen atmosphere is needed to reduce by-products, such as Li_2CO_3 and LiOH. In addition, the evaporation of the electrolyte is another challenge in the performance of Li-O_2 batteries [5–7]. In terms of improving reaction activity and reducing overpotential, designing efficient catalysts is an effective strategy [8–12]. However, irreversible loss, such as the volatilization and decomposition of electrolytes, and the side reaction with other air components will occur during the reaction process in the open system [13–17]. From the point of practical applications, an O_2 tank supplier not only occupies a large space but also decreases the specific energy density. Moreover, if the air is applied to replace the high-purity O_2, these substances (Li_2CO_3 and LiOH) are not easily decomposed, resulting in irreversible capacity damage to the battery. Therefore, a new design of a closed lithium–oxygen battery without a continuous oxygen supplier is promising for practical application in the future.

The design idea of the closed battery is to quantitatively control the reactants and discharge products and eliminate the participation of gaseous oxygen. As for the electrochemical reaction mechanism of Li-O_2, some studies have proposed that Li first reacts

with O_2 to form metastable LiO_2 and subsequently transfers to Li_2O_2 through a second reduction or disproportionation, as shown in Equations (1)–(3) [6,18,19]. The LiO_2 in the first step reaction is quite unstable. Even without the presence of O_2, lithium superoxide (LiO_2) can be further reacted to form peroxide (Li_2O_2) (Equation (2)). When the reaction rate is prolonged, a disproportionation reaction (Equation (3)) occurs in the discharge of superoxide (LiO_2) which converts to oxygen and peroxide (Li_2O_2) [6,20–24]. Hence, maintaining the stable existence of superoxide as a reactant is the most crucial issue in a closed battery.

$$O_2 + Li^+ + e^- = LiO_2 \quad (1)$$

$$LiO_2 + Li^+ + e^- = Li_2O_2 \quad (2)$$

$$2LiO_2 = Li_2O_2 + O_2 \quad (3)$$

Recently, Kang et al. pointed out in a review [25] that the surrounding conditions, i.e., electrolytes, redox mediators, and catalysts, had a significant effect on the stability of intermediate LiO_2 [10,26–29]. Lu et al. stabilized the formation of LiO_2 using Ir-rGO as the cathode catalyst [27]. In general, Li-O_2 batteries have been studied because the reaction path is affected by specific electrolytes, additives, and catalysts, which will change the reaction product, reduce the polarization potential, and improve the rate performance [30–34]. Our groups have successfully cycled an amorphous LiO_2-based Li-O_2 battery with a Pd-rGO hybrid catalyst [26]. This battery showed an ultra-low overpotential (~0.3 V), long cycle life, and high-rate capability. However, in this amorphous LiO_2-based Li-O_2 battery, O_2 is still necessary to keep this electrochemical reaction. Just recently, Zhou's group reported a high energy density and a long-life lithium-ion battery based on the conversion of Li_2O to Li_2O_2 [35]. Due to concerns that oxygen leakage will affect battery performance, Zhou's group gave up the 480 mAh g^{-1} capacity of Li_2O to Li_2O_2. However, in our work, we improved the closed-type battery and proved that this part of the capacity has application value.

Taking advantage of the stabilization of amorphous LiO_2 in our previous work, we propose to build a closed-type lithium–oxygen battery whose electrochemical reaction is mainly based on the conversion of LiO_2 and Li_2O_2 ($LiO_2 + e^- + Li^+ \leftrightarrow Li_2O_2$). Compared with our previous work, this process extends the reversible cycle of a closed battery from LiO_2 to the Li_2O_2 stage without gaseous oxygen [26]. The results indicate that the closed lithium–oxygen battery tested according to this strategy reached 57 cycles at a current density of 500 mA g^{-1}. At the same time, we quantified the amount of oxygen released during the lithium superoxide phase by DEMS. In this work, the proposed new concept of a closed "Li-O_2" battery system opens up a new avenue for the battery while promoting the application of catalysts and batteries based on the conversion of LiO_2 and Li_2O_2.

2. Results and Discussion

The closed "Li-O_2" batteries require stable lithium superoxide to participate in the reaction. To obtain the reactant lithium superoxide, we prepared Pd-rGO catalysts with Pd clusters by hydrothermal methods. As shown in Figure S1a, scanning electron microscope (SEM) images show that the synthesized Pd-rGO has a wrinkled 2D sheets structure of graphene. The diameter of the sheets is greater than 1 μm. In Figure S1b,c, the transmission electron microscope (TEM) shows about 5 nm of diameter palladium (Pd) particles. Corresponding to the XRD spectrum in Figure S1d, the characteristic peaks of the Pd at 40.118°, 46.658°, and 68.119° can be indexed to PDF#46-1043. The broad peak at about 21.8° corresponded to rGO.

The depth of discharge is an essential parameter for the reversible cycle of a closed battery. As shown in Figure 1 and Table 1, we use a unique catalyst (Pd-rGO) to pre-discharge (688 mAh g^{-1}) to control the cathode deposition product at the lithium superoxide stage. (This step can also be taken as an activation process.) Then, the O_2 supplier is shut off, and the battery is limited to 480 mAh g^{-1} for discharge and charge cycles. This electrochemical reaction is mainly based on the conversion of LiO_2 and Li_2O_2 ($LiO_2 + e^- + Li^+ \leftrightarrow Li_2O_2$).

The battery is assembled, as we reported in a previous publication. The catalyst is loaded on carbon paper as a cathode and assembled into a battery for the pre-discharge test. After pre-discharge, the battery is sealed to maintain a closed environment. According to literature reports and theoretical capacity calculations (Table 1), it is determined that the theoretical capacity corresponding to LiO_2 is 688 mAh g^{-1} [36]. The theoretical capacity for the conversion from LiO_2 to Li_2O_2 is 480 mAh g^{-1}. Therefore, the battery is limited to a specific capacity of 688 mAh g^{-1} for pre-discharge, and the specific capacity of the cycle is limited to 480 mAh g^{-1}.

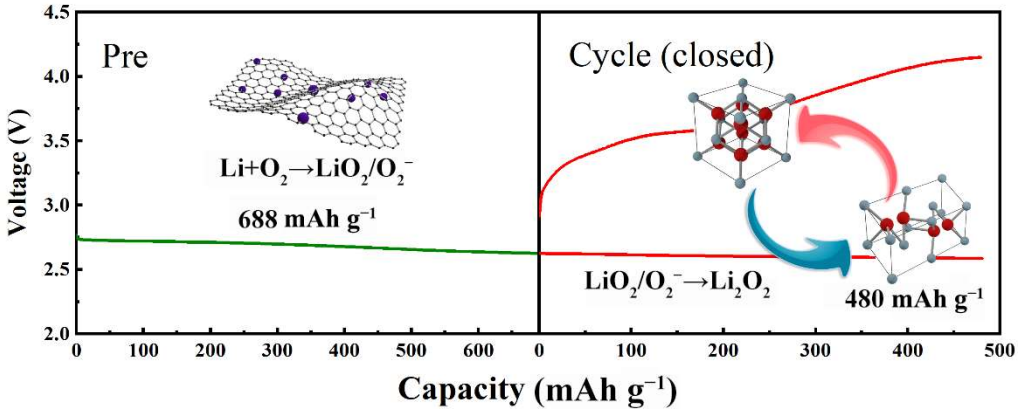

Figure 1. Schematic representations of a closed "Li–O_2" battery based on the conversion of LiO_2 and Li_2O_2 ($LiO_2 + e^- + Li^+ \leftrightarrow Li_2O_2$).

Table 1. The theoretical discharge capacity of three reaction paths.

	Process	Theoretical Specific Capacity (mAh g^{-1})
$O_2 + Li^+ + e^- \rightarrow LiO_2$	Pre-Discharge	688.4021
$O_2 + 2Li^+ + e^- \rightarrow Li_2O_2$	Open-Discharge (With O_2)	1168.5377
$LiO_2 \rightarrow Li_2O_2$	Closed-Cycle (No O_2)	480.1356

Then, the charge–discharge cycle performance of closed batteries was tested at different current densities. As shown in Figure 2a, the batteries discharged and charged with a current density of 100, 200, and 500 mA g^{-1}, respectively. At 200 mA g^{-1}, the charging potential of the battery was stable at 3.2 V. After the charging specific capacity reached 400 mAh g^{-1}, the potential gradually increased to 4.1 V. At a current density of 500 mA g^{-1}, the charging voltage gradually increases to 4.2 V. At a lower current density (100 mA g^{-1}), the polarization potential (4.4 V) is higher than the high current density (200 or 500 mA g^{-1}). This is because the charging time for low current density is longer, and the disproportionation reaction of the generated lithium superoxide to lithium peroxide is more pronounced. To demonstrate the importance of Pd cluster catalysts in closed batteries, the blank control group is rGO as a catalyst. In Figure 2b, the charging voltage of 100 mA g^{-1} has reached 4.4 V, and it can't even be fully charged to 480 mAh g^{-1} at high current density. It demonstrates that the electrocatalytic activity of rGO is relatively weak. With the number of cycles increasing, the discharge platform is unchanged, but the charging potential increases. As shown in Figure 2c, the charging potential of the first cycle is 4.2 V, and the charging potential rises to 4.4 V after 50 cycles. Meanwhile, the discharge platform is reduced from 2.6 V to 2.4 V. It may be attributed to the continuous accumulation of side reactions, the electrolyte's decomposition, and the catalyst's deactivation. Figure 2d shows the long-cycle performance of closed batteries. At different current densities of 100, 200, and 500 mA g^{-1}, the closed Li-O_2 battery can be cycled to 20, 39, and 57 cycles, respectively.

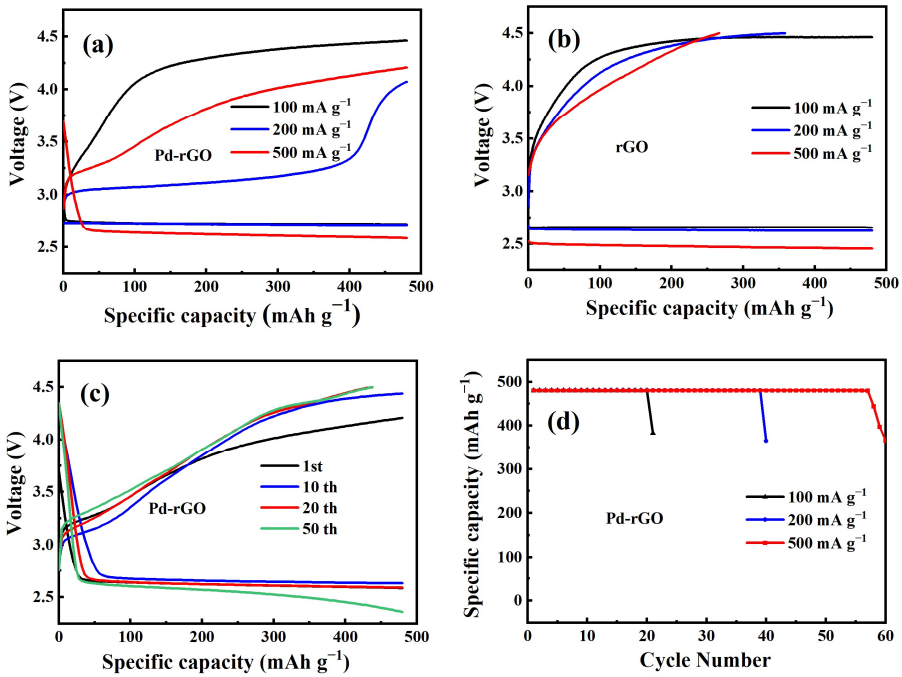

Figure 2. The specific capacity is cut off at 480 mAh g^{-1}. The first cycle charge and discharge curves at 100, 200, 500 mA g^{-1}; (**a**) Pd–rGO for Li–O_2 battery; (**b**) rGO for Li–O_2 battery; (**c**) the dis–charge/charge curves at different cycles of Pd–rGO for Li–O_2 battery at 500 mA g^{-1}; (**d**) the cycle performances of Pd–rGO and rGO for Li–O_2 battery at different current density.

To verify the reversibility of the closed battery, the production, decomposition, and change of the products during the charge and discharge processes of the lithium–oxygen battery can be detected by the in situ Raman spectrum. The battery is charged and discharged at a current density of 200 mA g^{-1}, and the Raman spectrum is collected every 20 min. These characteristic peaks correspond to Li_2O_2 and O_2^- at 790–805 cm^{-1} and 1085–1105 cm^{-1}, respectively [36–39]. After discharge, the signal peak of Li_2O_2 can be observed gradually, as shown in Figure 3a. The map of Figure 3b shows the signal changes more intuitively. As the depth of the discharge process occurs, the signals of Li_2O_2 increase. This indicates that the process of the discharge reaction corresponds to Equation (2). During the charging process, the Li_2O_2 signal (790–805 cm^{-1}) gradually disappears and the O_2^- (1085–1105 cm^{-1}) signal increases. It proves that the entire cycle is reversible. Moreover, Equation (3) is a side reaction usually accompanied by oxygen release, which should be avoided in practical applications.

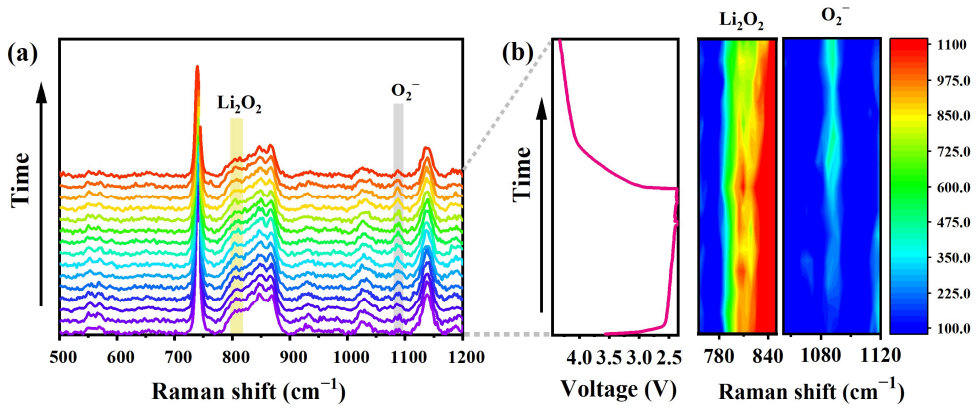

Figure 3. The in situ Raman spectrum of Pd–rGO catalyzed for Li–O_2 battery. (**a**) The in situ Raman overlay graph. (**b**) The in situ Raman mapping and corresponding voltage curves.

In addition to Raman, UV–Vis spectroscopy is also a method to detect lithium peroxide. In Figure S2, UV–Vis spectroscopy can characterize the changes in Li_2O_2 in batteries. To confirm the conversion reaction of LiO_2 to Li_2O_2 in a closed Li-O_2 battery, we immersed cathodes with different specific capacity discharges in a mixed solution of $TiOSO_4/H_2SO_4$ reagent and sulfuric acid. Then, the presence of lithium peroxide was measured by UV–Vis. In Figure S2, the Li_2O_2 cannot be observed at a pre-discharge. The signal of Li_2O_2 appears during closed discharge and disappears after closed charge. It verifies that LiO_2 can be obtained by pre-discharge, and the product is converted reversibly between LiO_2 and Li_2O_2 during the redox reaction process of the battery.

The EQCM is an intuitive way to characterize the production and decomposition of solid-phase products LiO_2 and Li_2O_2. The results of the EQCM are shown in Figure 4. The orange squares are the data points of the mass change, and the green lines are the corresponding fitted curves. In the process of stable discharge, the mass has a linear relationship with the capacity. The EQCM theoretical slope table of different test environments and related products is shown in Table 2. After completing the pre-discharge in O_2, we remove the O_2 and simulate a closed oxygen-free environment with an Ar atmosphere. The discharge and charge cycle data are shown in Figure 4a,b. The slope values of the mass change during discharge and charge are 2.05 ng nAh^{-1} and 2.12 ng nAh^{-1}, respectively. The theoretical slope for converting LiO_2 to Li_2O_2 is 2.08 ng nAh^{-1}. The slope value of the Pd-rGO in Ar is very close to the theoretical slope value of the conversion of lithium LiO_2 to Li_2O_2. This corresponds to the single electron conversion process in the closed Pd-rGO battery. In addition, the Li-O_2 battery with rGO in oxygen was used as a control group (Figure 4c,d). The slope of the product mass and capacity of the rGO battery (0.34 ng nAh^{-1}) is lower than the theoretical slope of O_2 to Li_2O_2 (0.855 ng nAh^{-1}). The slope of the battery with rGO in O_2 is close to the theoretical slope of O_2 to LiOH. This shows that the discharge process of this battery is a multi-electron process.

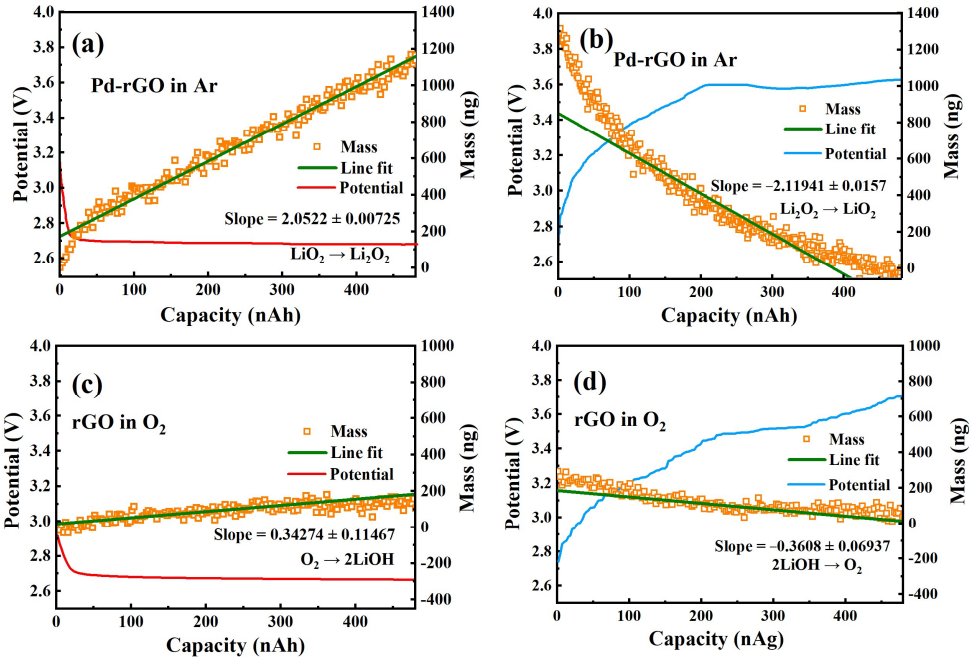

Figure 4. Mass change of Ti film quartz crystal in the LiTFSI/TEGDME electrolyte at a 1 μA. (**a**,**b**) Discharge and charge curves and mass changes of Li-O_2 battery with Pd–rGO as a catalyst in Ar (simulate closed battery status). (**c**,**d**) Discharge and charge curves and mass changes of Li –O_2 battery with rGO as a catalyst in O_2 (simulate open Li-O_2 battery status).

Table 2. The EQCM experimental matrix of different products.

	M (mol·g^{-1})	N (mol)	C (mAh g^{-1})	1/C (ng nAh^{-1})
LiO_2	38.9388	1	688.4021	1.4526
Li_2O_2	45.8788	2	1168.5377	0.8558
2LiOH	47.8946	4	2238.7083	0.4467
$LiO_2 \rightarrow Li_2O_2$	6.9400	1	480.1356	2.0827
Pd-rGO in Ar				2.0522
rGO in O_2				0.3427

Faraday's laws of electrolysis: C = nF/3.6 M; C: theoretical capacity; n: the number of electrons transferred; F: Faraday's constant (F = 96485 C mol^{-1}); M: molar mass; n: the number of electrons transferred; 1/C: the reciprocal of theoretical capacity is the slope in the EQCM.

To detect the gas changes and determine whether oxygen was released in the Pd-rGO closed battery, the electrochemical mass spectrometry (DEMS) was tested at 200 μA. First, the battery was pre-discharging under an O_2/Ar mixed gas. As shown in Figure 5a,d, the pre-discharge O_2 consumption is stable and linearly related to the capacity. After calculation, the number of electron transfers corresponding to oxygen consumption is 1.06 e^-/O_2. It indicates that the discharge product formed by the pre-discharge is LiO_2. Then, the closed system is tested in a pure Ar environment. In theory, the reaction of the Pd-rGO closed battery is from LiO_2 to Li_2O_2. This charging process is a reverse reaction with no oxygen released. However, in Figure 5c, we detected a small amount of O_2 release during the charging phase. According to calculations, the reaction for the decomposition and release of oxygen by LiO_2 accounts for about 16.32% (Figure 5f and Table 3). Correspondingly, in Figure 5b,e, the discharge process is accompanied by an approximate amount of oxygen consumption. After the oxygen supply is stopped, it is difficult to quickly remove the small amount of oxygen remaining in the battery. Therefore, part of the reaction of Equation (1) is mixed into the closing process.

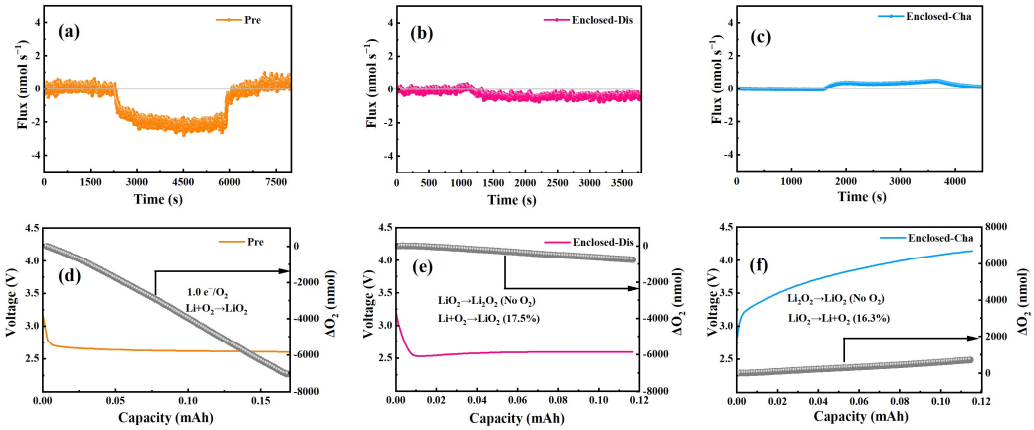

Figure 5. DEMS analyses in Pd–rGO closed battery. The amount of O_2 consumed and released in different processes: (**a**) pre–discharge; (**b**) closed–discharge; (**c**) closed–charge; (**d**–**f**) is the corre–sponding gas and capacitance curve.

Table 3. DEMS data of a Pd-rGO closed battery.

Sample	ΔQ (e$^-$)	ΔO_2 (nmol)	n (e$^-$ mol^{-1})
Closed Pre	7.46×10^{-6}	7053.46 ($O_2 \rightarrow LiO_2$)	1.06
Closed Discharge	0.76×10^{-6}	762.06 ($O_2 \rightarrow LiO_2$)	1.00
Closed Charge	0.71×10^{-6}	711.06 ($LiO_2 \rightarrow O_2$)	1.00

Number of electron transfers: $n = \Delta Q/\Delta O_2$; Q: total number of electrons.

The electrochemical performance of Pd-rGO in O_2 and Pd-rGO closed batteries were examined in 2025-type Li-O_2 batteries, as shown in Figure 6. From the cyclic voltammetry

curves, it can conclude that the reaction is different between a closed system battery and an unclosed (pre-discharged) battery. As shown in Figure S3, the Pd-rGO-based Li-O_2 battery exhibits a superior OER and ORR performance compared to the closed battery, with significant reduction peaks and oxidation peaks at 2.5 V and 3.4 V, respectively. This indicates that the reaction of the catalyst Pd-rGO in the pre-discharge process is based on O_2/O_2^-. The decomposition process of the toroids Li_2O_2 produces a higher overpotential, while the film-like LiO_2 has a lower overpotential [20,40]. Therefore, the Pd-rGO closed battery needs a higher charging potential to decompose Li_2O_2.

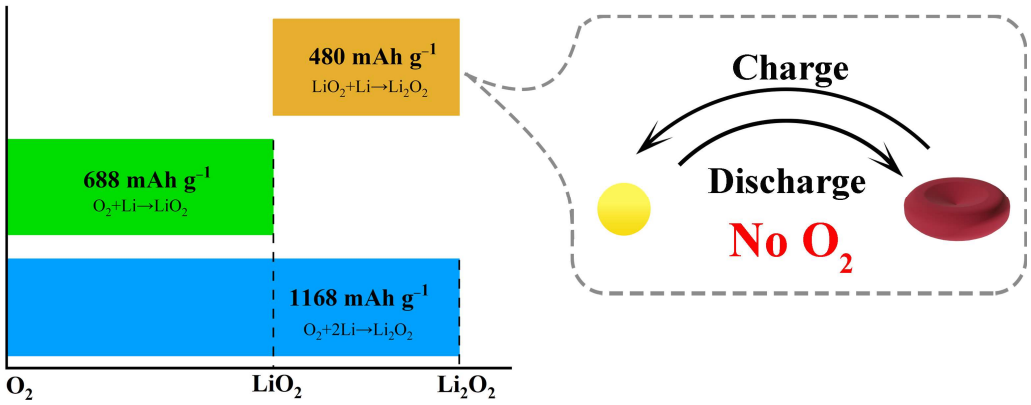

Figure 6. Batteries have two different stages of discharge products: LiO_2 and Li_2O_2. The conversion from LiO_2 to Li_2O_2 does not require O_2. This can realize the reversible cycle of a closed battery with a capacity of 480 mAh g^{-1}.

3. Materials and Methods

3.1. Synthesis of a Pd-rGO Hybrid Catalyst

A Pd-rGO hybrid catalyst is synthesized by a hydrothermal method [26]. In a typical process, 15 mL of GO suspension (5.6 mg/mL) and 5 ml of Pd solution ($PdCl_2$ 8.47 mg) were dispersed in 60 mL of deionized water, sonicated overnight, and stirred for 2 h. A total of 5 mL of hydrazine hydrate solution with a concentration of 85% was added dropwise to the suspension and stirred vigorously for 30 min. The mixed solution was poured into a stainless steel reaction kettle and heated at 180 °C for 12 h. After cooling to room temperature, it was separately centrifuged and washed twice with water and ethanol, and the solid product was freeze-dried for 24 h. The powder sample was placed in a tube furnace filled with an Ar atmosphere and heated at 400 °C for 1 h.

The control sample rGO was prepared in the same way without adding the Pd solution.

3.2. Structure Characterization of a Pd-rGO Catalyst

A Rigaku Smartlab powder diffractometer measured powder X-ray diffraction (XRD) with 2θ ranging from 10° to 80° and Cu Ka radiation (λ = 0.154 nm, 9 kW). The morphologies of Pd-rGO were observed on a scanning electron microscope (SEM SU8010 HITACHI) and transmission electron microscopy (TEM HT7700-Ex HITACHI). The acceleration voltage of SEM was 5 kV, 10 uA, with a work distance of 8 mm. The acceleration voltage of TEM was 100 kV.

3.3. Battery Fabrication and Electrochemical Measurements

The battery uses lithium metal as the negative electrode, and Pd-rGO (0.3 mg) loaded carbon paper (Torray) is the positive electrode. The separator is the glass filter separator (Whatsman). The cycle test of the closed battery uses a CR2025 coin cell. The electrolyte was a 1.0 M LITFSI/TEGDME solution with a water content of less than 50 ppm. The positive electrode was added dropwise with a slurry mixed from a dry sample, super p, and PVDF at a mass ratio of 4:4:2, and then dispersed in the NMP solution. A sample loaded with a mixture of super P and PVDF (8:2) was used as the control group. The porous cathode

was dried under a vacuum at 120 °C for 12 h. The batteries were assembled in an argon-filled glove box with a water and oxygen content of less than 0.1 ppm. Electrochemical measurements were carried out on the LAND CT2001 battery tester system. The charge and discharge window are controlled at 2 V to 4.5 V. The battery was pre-discharged to 688 mAh g^{-1} in oxygen. Then, the cathode diffusion hole was sealed by aluminum foil, and the battery was cycled at 480 mAh g^{-1} in an oxygen-free environment. The cyclic voltammetry (CV) measurements were performed on a PRINCETON PMC-2000 electrochemical workstation.

The spectrophotometric method was used to detect the existence of Li_2O_2. The UV–Vis spectrum was carried out on Agilent Cary 60 UV–Vis with wavelengths ranging from 350 to 800 nm. A total of 10 g of Ti(IV)OSO_4 was first dissolved in 500 mL of 1 M H_2SO_4 and filtered to obtain a settled solution. A total of 2.26 g of Li_2O_2 was then added to 10 mL of $TiOSO_4/H_2SO_4$. 0.5, 1, 1.5, 2, and 2.5 mL of that solution were attenuated to 5 mL to obtain slandered samples. As for the spectrum of the cathode, the discharged/charged cathode was first encapsulated into a 10 mL glass penicillin bottle in the glove box. A total of 5 mL of $TiOSO_4/H_2SO_4$ was injured into the bottle. After 15 min of shocking, the liquid in the bottle was used for UV testing. Raman spectra were obtained with a Renishaw inVia confocal Raman microscope with an excitation wavelength of 532 nm ranging from 600 to 2000 cm^{-1}. DEMS was performed on an OmniStar GSD 320.

Electrochemical quartz crystal microbalance (EQCM) analyses were performed on a QCM922A-010 and PRINCETON PMC-2000. A Ti film quartz crystal (AT-cut 9 MHz) loaded with Pd-rGO or Super-P (<0.1 mg) was the working electrode. A platinum electrode coated with $LiFePO_4$ was the counter electrode and reference electrode. The electrolyte was a 1.0 M LITFSI/TEGDME solution with a water content of less than 50 ppm. Before the experiment, the electrolyte was injected into Ar gas for 30 min. The environment of O_2 and Ar is provided by pre-injecting 15 min of O_2 or Ar into the electrolyte while maintaining the flow of oxygen and argon during charging and discharging.

4. Conclusions

In summary, we report a closed-type lithium–oxygen battery model based on the conversion between LiO_2 and Li_2O_2. This conversion process has been analyzed by in situ Raman spectra, UV–Vis, electrochemical quartz crystal microbalance, and DEMS. At a current density of 500 mA g^{-1}, the closed lithium–oxygen battery with Pd-rGO as a catalyst can be cycled more than 57 times. Hence, this work provides new insights and the possibility for further research and commercial applications of lithium–oxygen batteries without O_2. Moreover, this strategy could also be applied to explore more highly efficient catalysts, electrolytes, and redox media in other batteries, such as Na-O_2 and Zn–air batteries.

Supplementary Materials: The following supporting information can be downloaded at https://www.mdpi.com/article/10.3390/inorganics11020069/s1. Figure S1. (a) SEM images of Pd-rGO; (b) and (c) TEM image and HRTEM of Pd-rGO, respectively; (d) the XRD patterns of Pd-rGO; Figure S2. UV–Vis of Pd-rGO Li-O_2 battery. Cathodes with different discharge-specific capacities are immersed in a mixed solution of $TiOSO_4/H_2SO_4$ reagent and sulfuric acid; Figure S3. CV curves of Pd-rGO tested in an O_2 environment and a closed battery in the LiTFSI/TEGDME electrolyte at a scan rate of 0.1 mV s^{-1}; Figure S4. The cycle data of rGO closed batteries at 500 mA g^{-1}.

Author Contributions: Conceptualization, R.G. and X.L.; methodology, J.W.; funding acquisition, X.L. All authors have read and agreed to the published version of the manuscript.

Funding: This research was funded by the Beijing Natural Science Foundation (grant No. 2182082), the National Natural Science Foundation of China (grants 11975238 and 11575192), the Scientific Instrument Developing Project (grant No. ZDKYYQ20170001), the International Partnership Program (grant No. 211211KYSB20170060), and the Strategic Priority Research Program (grant No. XDB28000000) of the Chinese Academy of Sciences. The Fundamental Research Funds also supported this work for the Central Universities.

Data Availability Statement: Not applicable.

Conflicts of Interest: The authors declare no conflict of interest.

References

1. Bruce, P.G.; Freunberger, S.A.; Hardwick, L.J.; Jean-Marie, T. Li-O_2 and Li-S batteries with high energy storage. *Nat. Mater.* **2011**, *11*, 19–29. [CrossRef] [PubMed]
2. Geng, D.; Ding, N.; Hor, T.A.; Chien, S.W.; Liu, Z.; Wuu, D.; Sun, X.; Zong, Y. From Lithium-Oxygen to Lithium-Air Batteries: Challenges and Opportunities. *Adv. Energy Mater.* **2016**, *6*, 1502164. [CrossRef]
3. Grande, L.; Paillard, E.; Hassoun, J.; Park, J.-B.; Lee, Y.-J.; Sun, Y.-K.; Passerini, S.; Scrosati, B. The lithium/air battery: Still an emerging system or a practical reality? *Adv. Mater.* **2015**, *27*, 784–800. [CrossRef] [PubMed]
4. Huang, Y.; Wang, Y.; Tang, C.; Wang, J.; Zhang, Q.; Wang, Y.; Zhang, J. Atomic Modulation and Structure Design of Carbons for Bifunctional Electrocatalysis in Metal–Air Batteries. *Adv. Mater.* **2019**, *31*, 1803800. [CrossRef]
5. Léon, A.; Fiedler, A.; Blum, M.; Benkert, A.; Meyer, F.; Yang, W.; Bär, M.; Scheiba, F.; Ehrenberg, H.; Weinhardt, L.; et al. Valence Electronic Structure of Li_2O_2, Li_2O, Li_2CO_3, and LiOH Probed by Soft X-ray Emission Spectroscopy. *J. Phys. Chem. C* **2017**, *121*, 5460–5466. [CrossRef]
6. Cui, Q.; Zhang, Y.; Ma, S.; Peng, Z. Li_2 O_2 oxidation: The charging reaction in the aprotic Li-O_2 batteries. *Sci. Bull.* **2015**, *60*, 1227–1234. [CrossRef]
7. Zhang, X.; Gong, Y.; Li, S.; Sun, C. Porous Perovskite $La_{0.6}Sr_{0.4}Co_{0.8}Mn_{0.2}O_3$ Nanofibers Loaded with RuO_2 Nanosheets as an Efficient and Durable Bifunctional Catalyst for Rechargeable Li–O_2 Batteries. *ACS Catal.* **2017**, *7*, 7737–7747. [CrossRef]
8. Ma, R.; Sasaki, T. Nanosheets of oxides and hydroxides: Ultimate 2D charge-bearing functional crystallites. *Adv. Mater.* **2010**, *22*, 5082–5104. [CrossRef]
9. Liu, Y.; Xiao, C.; Li, Z.; Xie, Y. Vacancy engineering for tuning electron and phonon structures of two-dimensional materials. *Adv. Energy Mater.* **2016**, *6*, 1600436. [CrossRef]
10. Lim, H.-D.; Lee, B.; Zheng, Y.; Hong, J.; Kim, J.; Gwon, H.; Ko, Y.; Lee, M.; Cho, K.; Kang, K. Rational design of redox mediators for advanced Li–O_2 batteries. *Nat. Energy* **2016**, *1*, 16066. Available online: https://www.nature.com/articles/nenergy201666#supplementary-information (accessed on 23 December 2015). [CrossRef]
11. Cheng, F.; Zhang, T.; Zhang, Y.; Du, J.; Han, X.; Chen, J. Enhancing electrocatalytic oxygen reduction on $MnO_{(2)}$ with vacancies. *Angew. Chem. Int. Ed. Engl.* **2013**, *52*, 2474–2477. [CrossRef] [PubMed]
12. Sun, C.; Li, F.; Ma, C.; Wang, Y.; Ren, Y.; Yang, W.; Ma, Z.; Li, J.; Chen, Y.; Kim, Y.; et al. Graphene–Co_3O_4 nanocomposite as an efficient bifunctional catalyst for lithium–air batteries. *J. Mater. Chem. A* **2014**, *2*, 7188–7196. [CrossRef]
13. Cheng, F.; Chen, J. Metal-air batteries: From oxygen reduction electrochemistry to cathode catalysts. *Chem. Soc. Rev.* **2012**, *41*, 2172–2192. [CrossRef] [PubMed]
14. Thotiyl, M.M.O.; Freunberger, S.A.; Peng, Z.; Bruce, P.G. The carbon electrode in nonaqueous Li-O_2 cells. *J. Am. Chem. Soc.* **2013**, *135*, 494–500. [CrossRef]
15. McCloskey, B.D.; Speidel, A.; Scheffler, R.; Miller, D.C.; Viswanathan, V.; Hummelshøj, J.S.; Nørskov, J.K.; Luntz, A.C. Twin Problems of Interfacial Carbonate Formation in Nonaqueous Li-O_2 Batteries. *J. Phys. Chem. Lett.* **2012**, *3*, 997–1001. [CrossRef]
16. Peng, Z.; Freunberger, S.A.; Chen, Y.; Bruce, P.G. A reversible and higher-rate Li-O_2 battery. *Science* **2012**, *337*, 563–566. [CrossRef]
17. Asadi, M.; Sayahpour, B.; Abbasi, P.; Ngo, A.T.; Karis, K.; Jokisaari, J.R.; Liu, C.; Narayanan, B.; Gerard, M.; Yasaei, P.; et al. A lithium–oxygen battery with a long cycle life in an air-like atmosphere. *Nature* **2018**, *555*, 502–506. [CrossRef]
18. Lu, Y.-C.; Gasteiger, H.A.; Crumlin, E.; McGuire, R., Jr.; Shao-Horn, Y. Electrocatalytic Activity Studies of Select Metal Surfaces and Implications in Li-Air Batteries. *J. Electrochem. Soc.* **2010**, *157*, A1016–A1025. [CrossRef]
19. Black, R.; Oh, S.H.; Lee, J.-H.; Yim, T.; Adams, B.; Nazar, L.F. Screening for superoxide reactivity in Li-O_2 batteries: Effect on Li_2O_2/LiOH crystallization. *J. Am. Chem. Soc.* **2012**, *134*, 2902–2905. [CrossRef]
20. Zhang, Y.; Zhang, X.; Wang, J.; McKee, W.C.; Xu, Y.; Peng, Z. Potential-Dependent Generation of O_2– and LiO_2 and Their Critical Roles in O_2 Reduction to Li_2O_2 in Aprotic Li–O_2 Batteries. *J. Phys. Chem. C* **2016**, *120*, 3690–3698. [CrossRef]
21. Peng, Z.; Chen, Y.; Bruce, P.G.; Xu, Y. Direct Detection of the Superoxide Anion as a Stable Intermediate in the Electroreduction of Oxygen in a Non-Aqueous Electrolyte Containing Phenol as a Proton Source. *Angew. Chem. Int. Ed. Engl.* **2015**, *54*, 8165–8168. [CrossRef] [PubMed]
22. Oh, S.H.; Black, R.; Pomerantseva, E.; Lee, J.-H.; Nazar, L. Synthesis of a metallic mesoporous pyrochlore as a catalyst for lithium-O_2 batteries. *Nat. Chem.* **2012**, *4*, 1004–1010. [CrossRef] [PubMed]
23. Yao, W.; Yuan, Y.; Tan, G.; Liu, C.; Cheng, M.; Yurkiv, V.; Bi, X.; Long, F.; Friedrich, C.R.; Mashayek, F.; et al. Tuning Li_2O_2 Formation Routes by Facet Engineering of MnO_2 Cathode Catalysts. *J. Am. Chem. Soc.* **2019**, *141*, 12832–12838. [CrossRef] [PubMed]
24. Gong, Y.; Ding, W.; Li, Z.; Su, R.; Zhang, X.; Wang, J.; Zhou, J.; Wang, Z.; Gao, Y.; Li, S.; et al. Inverse Spinel Cobalt–Iron Oxide and N-Doped Graphene Composite as an Efficient and Durable Bifuctional Catalyst for Li–O_2 Batteries. *ACS Catal.* **2018**, *8*, 4082–4090. [CrossRef]
25. Lim, H.-D.; Lee, B.; Bae, Y.; Park, H.; Ko, Y.; Kim, H.; Kim, J.; Kang, K. Reaction chemistry in rechargeable Li-O_2 batteries. *Chem. Soc. Rev.* **2017**, *46*, 2873–2888. [CrossRef]

26. Gao, R.; Liang, X.; Yin, P.; Wang, J.; Lee, Y.L.; Hu, Z.; Liu, X. An amorphous LiO_2-based Li-O_2 battery with low overpotential and high rate capability. *Nano Energy* **2017**, *41*, 535–542. [CrossRef]
27. Lu, J.; Lee, Y.J.; Luo, X.; Lau, K.C.; Asadi, M.; Wang, H.-H.; Brombosz, S.; Wen, J.; Zhai, D.; Chen, Z.; et al. A lithium-oxygen battery based on lithium superoxide. *Nature* **2016**, *529*, 377–382. [CrossRef]
28. Gao, X.; Chen, Y.; Johnson, L.R.; Jovanov, Z.P.; Bruce, P.G. A rechargeable lithium–oxygen battery with dual mediators stabilizing the carbon cathode. *Nat. Energy* **2017**, *2*, 17118. [CrossRef]
29. Li, F.; Tang, D.-M.; Chen, Y.; Golberg, D.; Kitaura, H.; Zhang, T.; Yamada, A.; Zhou, H. Ru/ITO: A carbon-free cathode for nonaqueous Li-O_2 battery. *Nano Lett.* **2013**, *13*, 4702–4707. [CrossRef]
30. Liu, T.; Leskes, M.; Yu, W.; Moore, A.J.; Zhou, L.; Bayley, P.M.; Kim, G.; Grey, C.P. Cycling Li-O_2 batteries via LiOH formation and decomposition. *Science* **2015**, *350*, 530–533. [CrossRef]
31. Khetan, A.; Luntz, A.; Viswanathan, V. Trade-Offs in Capacity and Rechargeability in Nonaqueous Li-O_2 Batteries: Solution-Driven Growth versus Nucleophilic Stability. *J. Phys. Chem. Lett.* **2015**, *6*, 1254–1259. [CrossRef] [PubMed]
32. Wu, S.; Tang, J.; Li, F.; Liu, X.; Yamauchi, Y.; Ishida, M.; Zhou, H. A Synergistic System for Lithium-Oxygen Batteries in Humid Atmosphere Integrating a Composite Cathode and a Hydrophobic Ionic Liquid-Based Electrolyte. *Adv. Funct. Mater.* **2016**, *26*, 3291–3298. [CrossRef]
33. Lutz, L.; Yin, W.; Grimaud, A.; Alves Dalla Corte, D.; Tang, M.; Johnson, L.; Azaceta, E.; Sarou-Kanian, V.; Naylor, A.J.; Hamad, S.; et al. Capacity Na–O_2 Batteries: Key Parameters for Solution-Mediated Discharge. *J. Phys. Chem. C* **2016**, *120*, 20068–20076. [CrossRef]
34. Gittleson, F.S.; Jones, R.E.; Ward, D.K.; Foster, M.E. Oxygen solubility and transport in Li–air battery electrolytes: Establishing criteria and strategies for electrolyte design. *Energ. Environ. Sci.* **2017**, *10*, 1167–1179. [CrossRef]
35. Qiao, Y.; Jiang, K.; Deng, H.; Zhou, H. A high-energy-density and long-life lithium-ion battery via reversible oxide–peroxide conversion. *Nat. Catal.* **2019**, *2*, 1035–1044. [CrossRef]
36. Han, X.-B.; Kannari, K.; Ye, S. In situ surface-enhanced Raman spectroscopy in Li–O_2 battery research. *Curr. Opin. Electrochem.* **2019**, *17*, 174–183. [CrossRef]
37. Lau, K.C.; Qiu, D.; Luo, X.; Greeley, J.; Curtiss, L.A.; Lu, J.; Amine, K. Theoretical Exploration of Various Lithium Peroxide Crystal Structures in a Li-Air Battery. *Energies* **2015**, *8*, 529–548. [CrossRef]
38. Johnson, L.; Li, C.; Liu, Z.; Chen, Y.; Freunberger, S.; Ashok, P.C.; Praveen, B.B.; Dholakia, K.; Tarascon, J.-M.; Bruce, P.G. The role of LiO_2 solubility in O_2 reduction in aprotic solvents and its consequences for Li-O_2 batteries. *Nat. Chem.* **2014**, *6*, 1091–1099. [CrossRef]
39. Qiao, Y.; He, Y.; Wu, S.; Jiang, K.; Li, X.; Guo, S.; He, P.; Zhou, H. MOF-Based Separator in an Li–O_2 Battery: An Effective Strategy to Restrain the Shuttling of Dual Redox Mediators. *ACS Energy Lett.* **2018**, *3*, 463–468. [CrossRef]
40. Peng, Z.; Freunberger, S.; Hardwick, L.; Chen, Y.; Giordani, V.; Bardé, F.; Novák, P.; Graham, D.; Tarascon, J.-M.; Bruce, P.G. Oxygen reactions in a non-aqueous Li+ electrolyte. *Angew. Chem. Int. Ed. Engl.* **2011**, *50*, 6351–6355. [CrossRef]